Journal of Solid State Chemistry **149,** 276–283 (2000)
doi:10.1006/jssc.1999.8527, available online at http://www.idealibrary.com on IDEAL®

EDS and TEM Study of the Family of Compounds with a Structure Based on $[Bi_{12}O_{14}]_\infty$ Columns in the Bi_2O_3–MoO_3 Binary System

Marielle Huvé,[1] Rose Noëlle Vannier, and Gaëtan Mairesse

Laboratoire de Cristallochimie et Physicochimie du Solide, ENSCL, B.P. 108, 59652 Villeneuve d'Ascq Cedex, France

Received March 24, 1999; in revised form September 15, 1999; accepted October 11, 1999

The family of compounds with a structure based on $[Bi_{12}O_{14}]_\infty$ columns in the Bi_2O_3–MoO_3 binary system was analyzed by EDS and studied by TEM. These observations confirm that this solid solution type is limited within the range $2.6 \leq Bi/Mo \leq 2.8$. The room temperature $Bi_{26}Mo_{10}O_{69}$ triclinic polymorph (Bi/Mo = 2.6) clearly differs from the monoclinic ones ($Bi_{26}Mo_{10}O_{69}$ at $T > 310°C$ and $Bi_{26}Mo_{9.6}Bi_{0.4}O_{68.4}$) by the doubling of the a period and the vanishing of a c glide plane. © 2000 Academic Press

Key Words: **bismuth; molybdenum; oxide; Bi_2O_3–MoO_3 binary system; $[Bi_{12}O_{14}]_\infty$ columns; EDS; TEM; electron dispersive spectroscopy; electron diffraction; high-resolution microscopy.**

INTRODUCTION

A new family of oxide anion conductors with a structure based on $[Bi_{12}O_{14}]_\infty$ columns was recently evidenced in the Bi_2O_3–MoO_3 binary system (1). According to Vannier *et al.*, it extends in the range $2.57 \leq Bi/Mo \leq 2.77$, and the parent compound of this series can be formulated $Bi_{26}Mo_{10}O_{69}$. For lower bismuth content a mixture with the Bi_2MoO_6 (Bi/Mo = 2) phase (2) was observed, and for higher bismuth content, the $Bi_{38}Mo_7O_{78}$ (Bi/Mo = 5.43) (3, 4) type phase was characterized. These results were confirmed by Buttrey *et al.* (5). However, the stoichiometry range was questioned by Enjalbert *et al.*, who proposed another compositional range, $2.86 \leq Bi/Mo \leq 3.50$, based on crystallographic statements (6).

The structure of these materials has been resolved in the $P2/c$ space group combining both X-ray and neutron diffraction data (1, 5, 7). It consists of covalent $[Bi_{12}O_{14}]_\infty$ columns connected with Bi, Mo, O species, in which the displacements of the oxygen atoms display unusually high values, likely correlated with some softness of this part of the structure which favors oxide anion mobility (Fig. 1). The oxygen diffusion takes place along the [010] direction, and these materials can therefore be considered the first monodimensional bismuth-based oxide anion conductors.

The actual symmetry of $Bi_{26}Mo_{10}O_{69}$ is triclinic with the following unit-cell parameters: $a = 11.800(4)$ Å, $b = 5.808(2)$ Å, $c = 24.744(2)$ Å, $\alpha = 89.85(2)°$, $\beta = 102.76(2)°$, and $\gamma = 89.97(2)°$. It undergoes a reversible transition to a monoclinic form around 310°C. The increase of bismuth content leads to the stabilization of this monoclinic form at room temperature by partial substitution for molybdenum with bismuth (Bi/Mo = 2.75 composition is monoclinic at room temperature). The crystal structure of the triclinic polymorph has not been resolved but seems closely related to that of the monoclinic one.

In a first step to confirm the solid solution domain and the structural characteristics of these materials, electron dispersive spectroscopy (EDS) was performed. Then in a second step, selected area electron diffraction (SAED) and high resolution electron microscopy (HREM) were carried out.

EXPERIMENTAL

The samples with Bi/Mo = 2.6, Bi/Mo = 2.75, and Bi/Mo = 3.30 composition were prepared according to the method previously described (1). To ascertain that there was no loss of starting reactants by volatilization, Bi/Mo = 2.60 and Bi/Mo = 2.75 were also prepared in sealed gold tubes. X-ray diffraction was used to check the purity.

Electron dispersive spectroscopy was performed on a Phillips CM30 transmission electron microscope operating at 300 kV and equipped with an energy-dispersive spectrometer (Tracor-Voyager) using a germanium detector and an ultrathin window to allow the detection of light elements, especially oxygen. Electron diffraction patterns and high-resolution images were obtained with Jeol 200CX and 4000EX microscopes with 1.7 Å point resolution. The powders were crushed and dispersed on a holed carbon film deposited on a copper grid. The computer-simulated HREM images were calculated using the EMS program (8).

[1] To whom correspondence should be addressed. Fax: +33 3 2043 6814. E-mail: huve@ensc-lille.fr.

0022-4596/00 $35.00

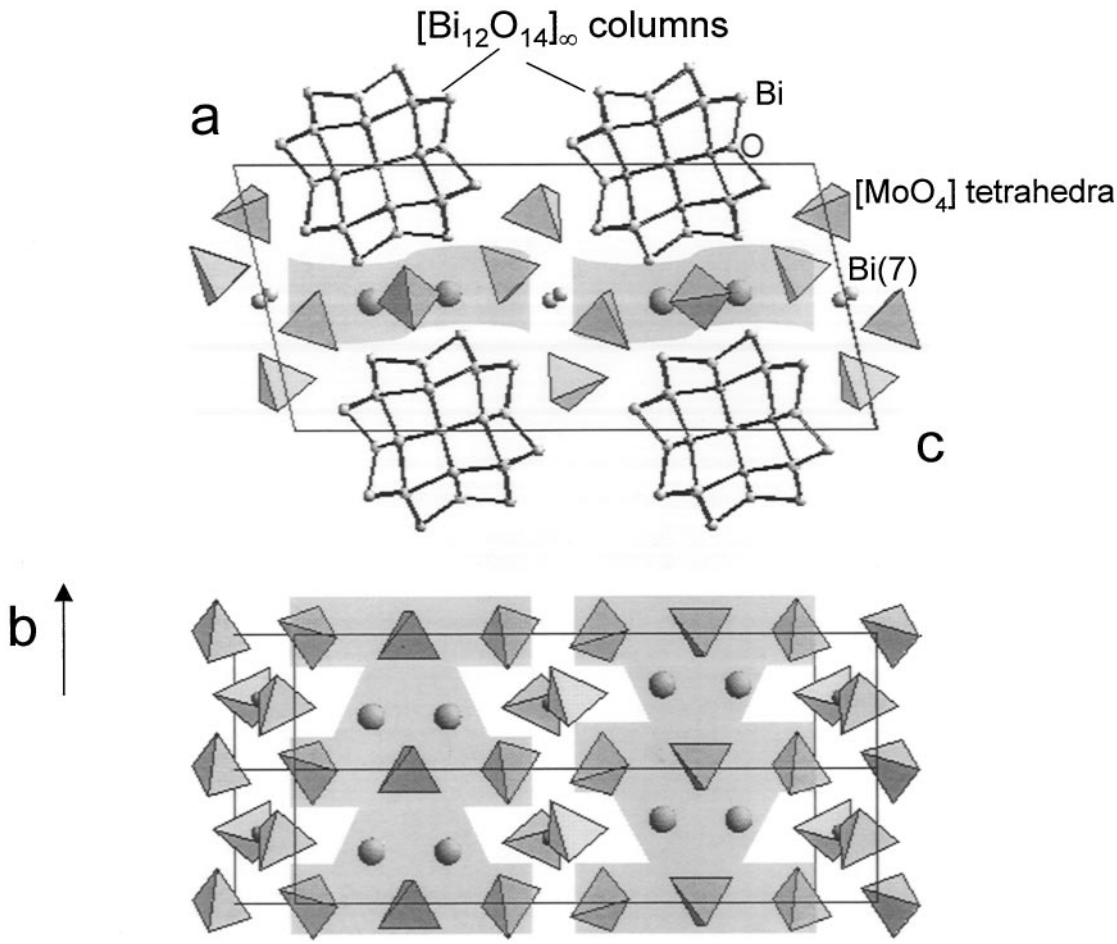

FIG. 1. $Bi_{26}Mo_{10}O_{69}$ structure: the shaded zones indicate the areas where oxygen diffusion is likely to take place.

RESULTS AND DISCUSSION

Electron Dispersive Spectroscopy Analysis

In electron dispersive spectroscopy the intensity emitted by the element is proportional to the concentration and to the thickness of the sample. Therefore, to perform quantitative analysis, Cliff and Laurimer $K_{x/O}$ factors (9) have to be known, as well as the thickness of each analyzed crystal. To determine the thickness of the crystals, the method developed by Van Capellen [10] is very interesting. The basic idea of this method is to adjust the thickness in order to reach the electroneutrality of the compound. The oxidation state of each cation is, of course, assumed to be known. The $K_{Bi/O}$ and $K_{Mo/O}$ factors of the program library were first precisely adjusted using crystals of Bi_2MoO_6 in which the stoichiometry is well defined.

Then, to determine the accuracy of this analysis, about 15 crystals of Bi_2MoO_6 were checked. The crystals were selected randomly, without consideration of morphology or dimension. The measurements gave rise to a Bi/Mo ratio of 1.97 ± 0.04. This is in very good agreement with the expected value of 2. Then the homogeneity and the nominal composition were proved when the average ratio of elements was close to this nominal composition with an accuracy of 5%.

$Bi_{26}Mo_{10}O_{69}$ Solid Solution Domain

To confirm the solid solution range proposed by Vannier *et al.* (1), electron dispersive spectroscopy analysis was performed on three compositions, two in the domain anounced by these authors with Bi/Mo = 2.60 and Bi/Mo = 2.75 nominal compositions and one out of this domain with Bi/Mo = 3.3 nominal ratio.

i. *Bi/Mo = 2.6 and Bi/Mo = 2.75 nominal composition.* This technique was therefore applied to powders with initial compositions Bi/Mo = 2.60 and Bi/Mo = 2.75,

TABLE 1
EDS Analysis

Bi/Mo (initial composition)	Bi/Mo (result of EDS analysis)	
2.00	1.97 (0.04)	
2.60[a]	2.66 (0.13)	
2.60[b]	2.67 (0.12)	
2.75[a]	2.79 (0.13)	
2.75[b]	2.77 (0.10)	
3.33[a]	2.72 (0.16)	5.02 (0.31)

[a] Synthesized in air.
[b] Synthesized in a sealed tube.

synthesized either in air or in sealed gold tubes. About 10 crystals were systematically analyzed, and the results are reported in Table 1. Their compositions were homogeneous and led to values close to the nominal ones. Moreover, those deduced for the materials synthesized in sealed tubes were very close to those synthesized in air, indicating that no significant loss of starting reactants occurred during the synthesis in air.

ii. *Bi/Mo = 3.3 nominal composition.* Although X-ray powder diffractograms clearly revealed that this composition was not a single phase, an analysis was performed. Twenty crystals were submitted to EDS analysis, and two groups of compositions were clearly distinguished: the first one (12 samples) exhibited a mean Bi/Mo ratio of 2.72 ± 0.16, very close to the upper limit of our composition range; the second one (the remaining eight samples) yielded a Bi/Mo ratio of 5.02 ± 0.31, close to the "$Bi_{38}Mo_7O_{78}$" (3, 4) formulation corresponding to the 5.43 expected value.

These quantitatively accurate analyses undoubtedly confirm that the solid solution is limited to the range $2.6 \leq Bi/Mo \leq 2.8$ and preclude the possibility of $Bi/Mo > 2.8$ compounds belonging to the structural type characterized by the existence of $[Bi_{12}O_{14}]_\infty$ columns, under our conditions of synthesis.

Electron Diffraction (SAED) and High-Resolution Electron Microscopy (HREM)

$Bi_{26}Mo_{10}O_{69}$ (Bi/Mo = 2.60) and $Bi_{26}Mo_{9.6}Bi_{0.4}O_{68.4}$ (Bi/Mo = 2.75) structures have been refined in the $P2/c$ space group using both X-ray (1) and neutron diffraction (5, 7). However, as evidenced by X-ray powder diffraction, the $Bi_{26}Mo_{10}O_{69}$ true symmetry is triclinic; it transforms reversibly to the closely related monoclinic form around 310°C. To compare these two polymorphs, electron diffraction and high-resolution electron microscopy experiments were performed on both compositions. As powders synthesized in sealed tubes gave rise to the same results, only data corresponding to the syntheses in air are reported.

Electron diffraction patterns corresponding to the [010], [100], and [001] zone axis, as well as a portion of the first Laüe zones, are reported in Figs. 2 and 3 for $Bi_{26}Mo_{9.6}Bi_{0.4}O_{68.4}$ and in Figs. 4 and 5 for $Bi_{26}Mo_{10}O_{69}$. These patterns are characterized by intense spots (arrows in Fig. 2a) related to a fluorite-type δBi_2O_3 subcell whose relationship to the $Bi_{26}Mo_{10}O_{69}$ supercell has already been clearly evidenced by Vannier *et al.* (7) and Ling *et al.* (11).

In the case of $Bi_{26}Mo_{9.6}Bi_{0.4}O_{68}$ (Figs. 2 and 3) $00l$, $l = 2n + 1$ reflections on the [100] electron diffraction pattern are due to the double diffraction effect since they are not present on the [010] electron diffraction pattern and do not question the space group. When tilting the [010] zone, the higher order Laüe zones appear (Fig. 3). The comparison between the zero-order and first-order Laüe zones, and in particular the comparison of the periodicity and shift between these two zones, leads to an extinction symbol $P1c1$ in accordance with (12) and compatible with the $P2/c$ space group of the structure. Indeed, there is no shift between these two zones, but the periodicity in the first-order Laüe zone is multiplied by two (in the reciprocal space) along the **c*** axis.

The electron diffraction patterns related to the triclinic $Bi_{26}Mo_{10}O_{69}$ form (Fig. 4) are closely related to those of the monoclinic bismuth-rich phase (Fig. 2). Obviously, the small triclinic distortion of the materials cannot be observed using this technique. At first glance, the [100] patterns are similar; however, a careful examination of the $Bi_{26}Mo_{10}O_{69}$ [010] and [001] patterns reveals extra spots (arrows in Fig. 4) along **a*** and **c***. The former are responsible for a superstructure involving a doubling of the **a** period. The latter are due to the disappearance of the **c** glide plane ($h0l$: $l = 2n$). Indeed in a comparison of the first and zero Laüe zones (Fig. 5) neither a periodicity difference nor a shift between these two zones appears. Thus the triclinic form clearly differs from the monoclinic one by a doubling of the **a** period and the absence of a **c** glide plane.

As evidenced by impedance spectroscopy and X-ray powder diffraction, $Bi_{26}Mo_{10}O_{69}$ reversibly transforms into the monoclinic form at about 310°C (1). Therefore, to complete this study, this compound was heated *in situ*, inside the microscope using a heating holder. The electron diffraction patterns obtained at about 300°C and room temperature are reported in Fig. 6. As expected at about 300°C, the extra spots observed in the triclinic form disappeared and gave rise to electron diffraction patterns similar to those observed for the monoclinic $Bi_{26}Mo_{9.6}Bi_{0.4}O_{68.4}$. On cooling, the initial patterns were recovered, proving the reversibility of this transformation.

To determine the structural difference between the triclinic and the monoclinic polymorphs, high-resolution

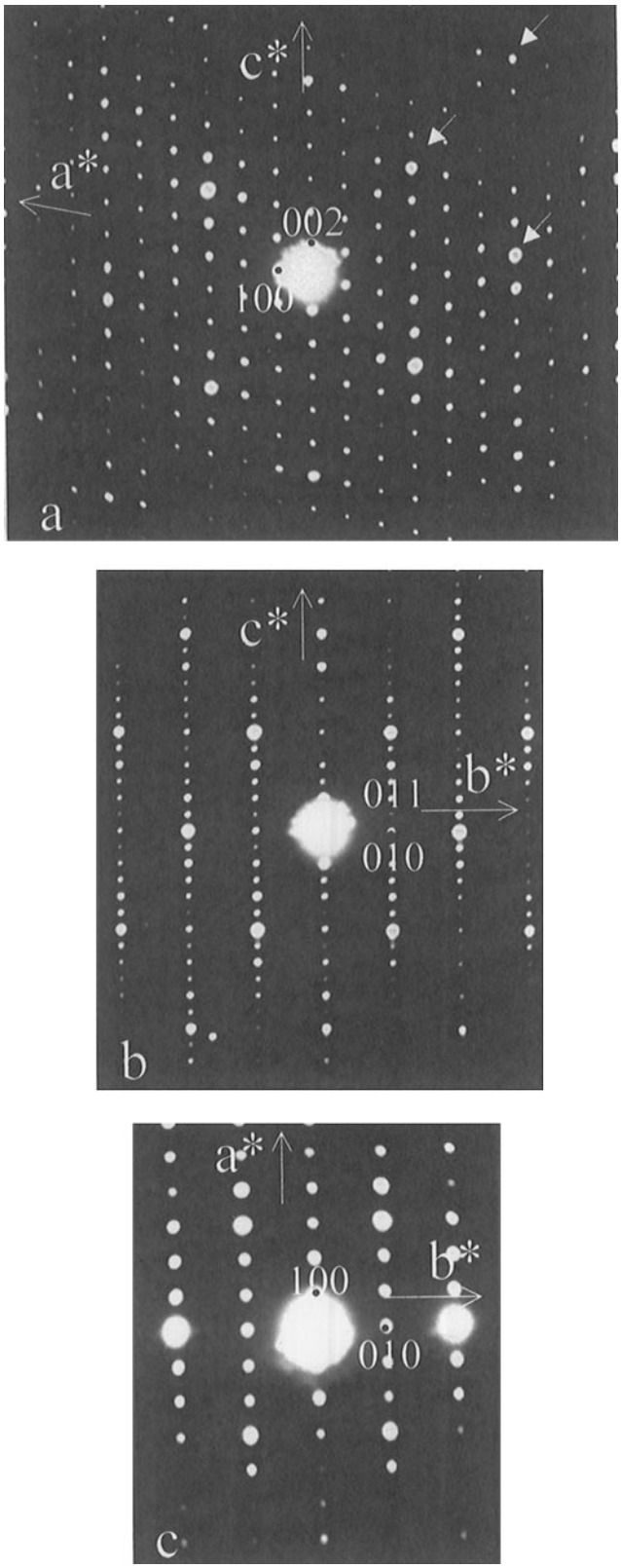

FIG. 2. $Bi_{26}Mo_{9.6}Bi_{0.4}O_{68.4}$: (a) [010]. (b) [100]. The $00l$, $l = 2n + 1$ reflections are due to double diffraction effects. (c) [001] electron diffraction patterns. The intense spots (arrows in a) are related to a fluorite-type δBi_2O_3 subcell.

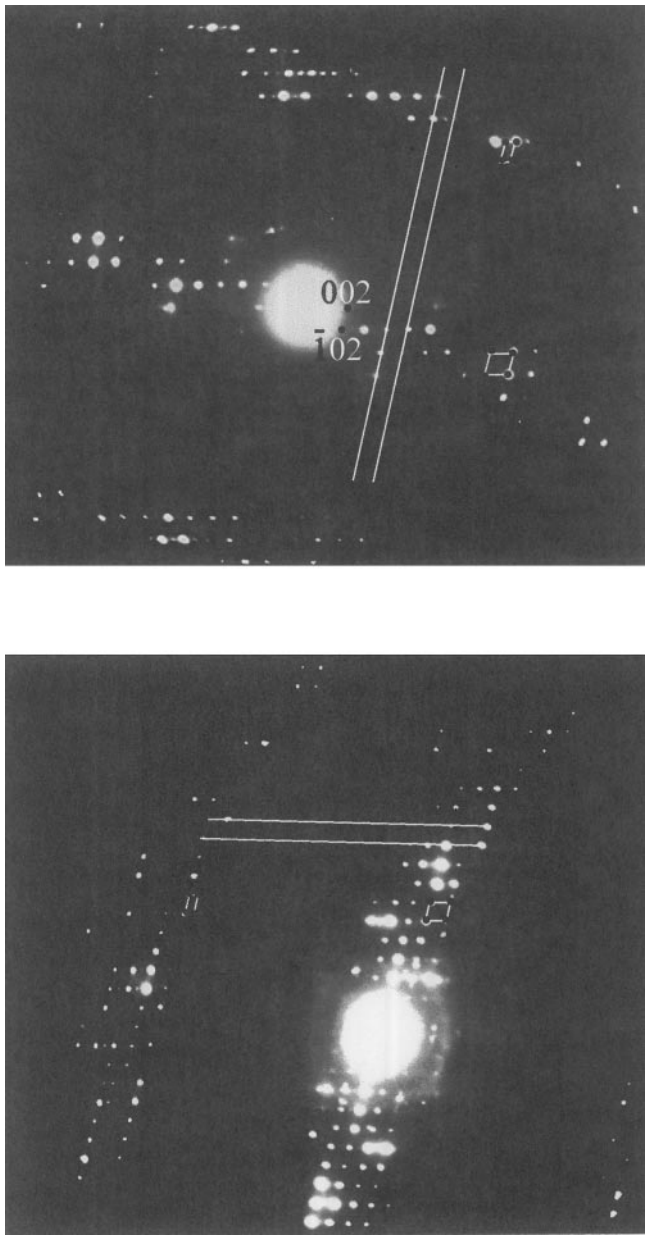

FIG. 3. $Bi_{26}Mo_{9.6}Bi_{0.4}O_{68.4}$: [010] zone axis pattern. The comparison of the periodicity and shift between these two zones leads to an extinction symbol $P1c1$ compatible with the $P2/c$ space group of the structure. Indeed, there is no shift between these two zones, but the periodicity in the first-order Laüe zone is multiplied by two (in the reciprocal space) along the **c*** axis.

electron microscopy was carried out. The more focused electron beam required by this technical method led to a local heating of the materials, and therefore, unfortunately, during the observation of $Bi_{26}Mo_{10}O_{69}$ we observed its gradual transformation to the monoclinic form. Therefore, the obtained images are very similar to those of the bismuth-rich compositions and correspond to the high-

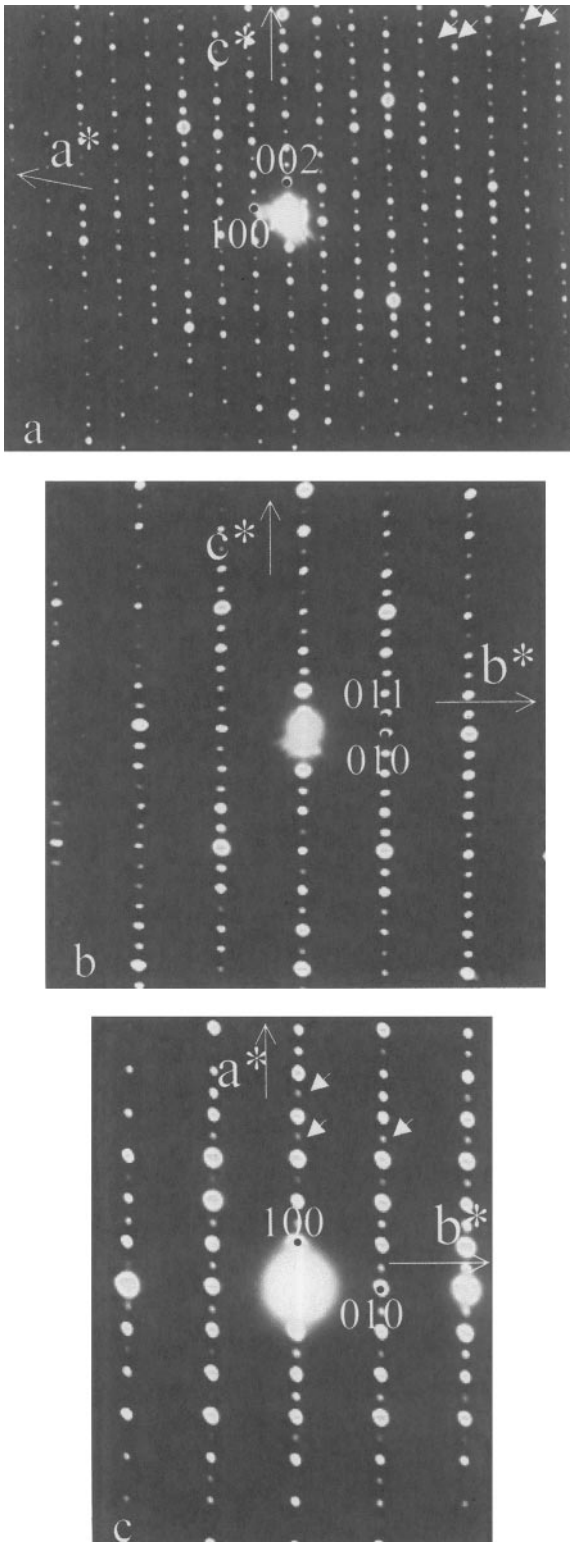

FIG. 4. $Bi_{26}Mo_{10}O_{69}$: (a) [010], (b) [100], and (c) [001] electron diffraction patterns. In the comparison to the electron diffraction of $Bi_{26}Mo_{9.6}Bi_{0.4}O_{68.4}$ (Fig. 2), extra spots (small arrows) appear along **a*** and along **c***. The former are responsible for a superstructure involving a doubling of the **a** period. The latter are due to the disappearance of the **c** glide plane, as we can see in Fig. 5. The indexation is given for the basic cell.

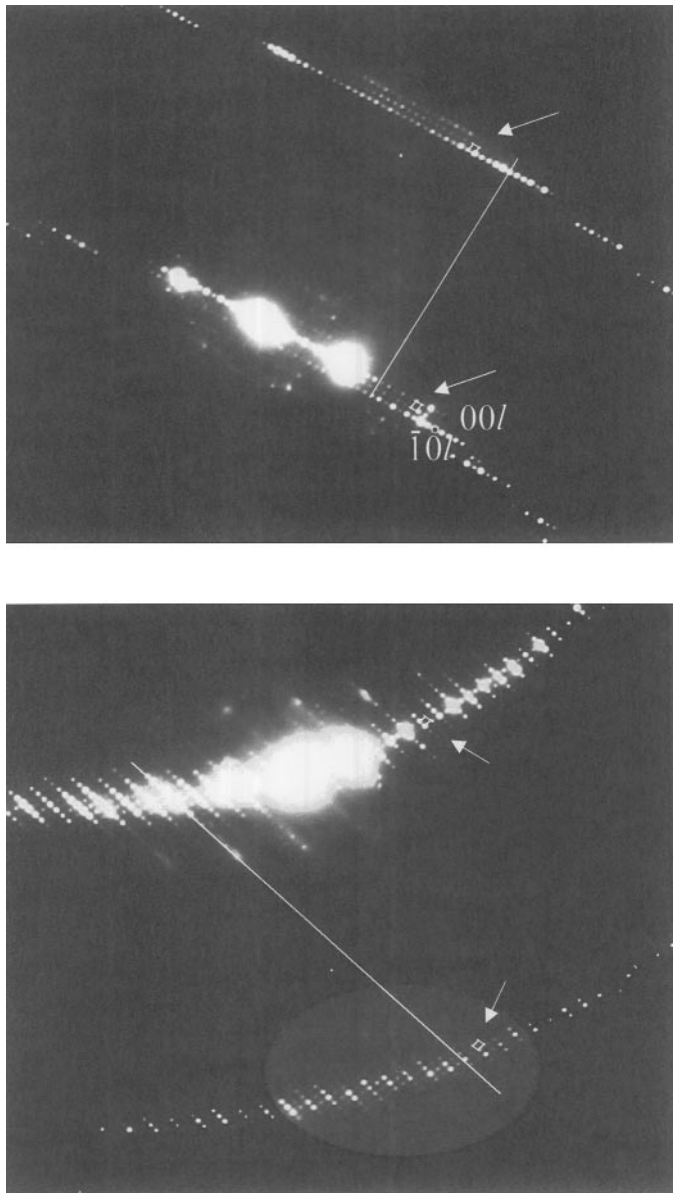

FIG. 5. $Bi_{26}Mo_{10}O_{69}$ [010] zone axis pattern. In the comparison to the $Bi_{26}Mo_{9.6}Bi_{0.4}O_{68.4}$ oxide the **a** doubling is observed. Neither a periodicity difference nor a shift between these two zones is observed that involves the disappearance of the **c** glide plane. The indexation is given for the basic cell.

temperature form of $Bi_{26}Mo_{10}O_{69}$. The [010] HREM image related to $Bi_{26}Mo_{9.6}Bi_{0.4}O_{68.4}$ is reported in Fig. 7a. It displays an excellent agreement with the calculated image using atomic positions reported in (7) (Fig. 7b). In this image, the correlation between atomic positions and contrast is not trivial: the cations appear as dark dots, and the positions of the Mo and one Bi (labeled Bi(7) in Fig. 1) are

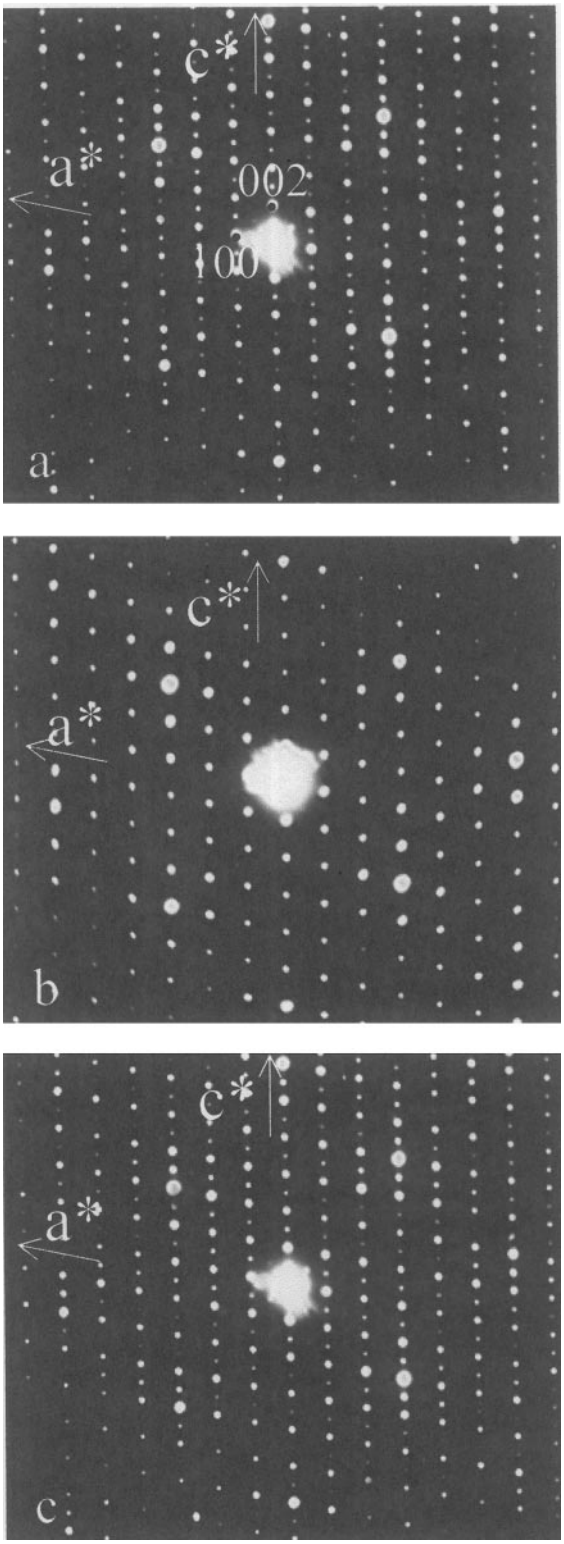

FIG. 6. $Bi_{26}Mo_{10}O_{69}$: the [010] electron diffraction patterns. (a) At room temperature. (b) At about 300°C. The extra spots responsible for the doubling of the **a** period as well as those along **c*** disappeared and gave rise to electron diffraction patterns similar to those observed for monoclinic $Bi_{26}Mo_{9.6}Bi_{0.4}O_{68.4}$ (Fig. 2). (c) On cooling, the initial patterns were recovered, proving the reversibility of this transformation.

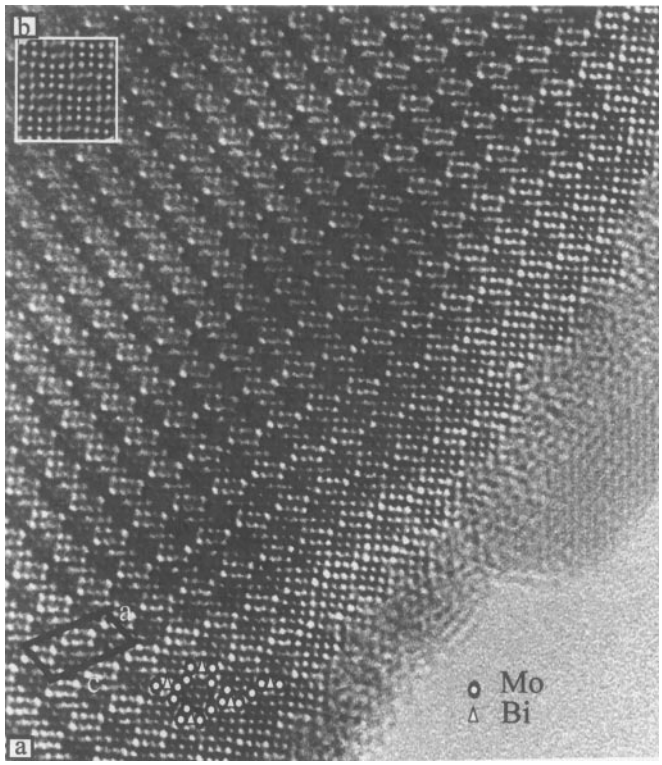

FIG. 7. $Bi_{26}Mo_{9.6}Bi_{0.4}O_{68.4}$. (a) The [010] high-resolution image. The cations appear as dark dots, and the positions of the Mo and one Bi (labeled Bi(7) in Fig. 1) are superimposed as circles and triangles. The other Bi positions are on the remaining dark dots. (b) An excellent agreement with the calculated image is observed.

superimposed as triangles and circles in Fig. 7. The other Bi positions are on the remaining dark dots. Some defects are often observed (arrows in Fig. 8a): they correspond to a twin boundary, and a schematic representation of this twin boundary is reported in Fig. 8b.

CONCLUSION

The limits of the $Bi_{26}Mo_{10}O_{69}$ type solid solution have been confirmed. It extends within the range $2.6 \leq Bi/Mo \leq 2.8$. The structure of the monoclinic form has been confirmed by HREM. The triclinic form is more complicated than a simple distortion of the monoclinic one. Moreover, this study revealed a doubling of the **a** period. As we did not manage to perform HREM on this polymorph, it is difficult to propose a structural model as yet. However, this structure exhibits isolated bismuth cations (labeled Bi(7) in Fig. 1), located around a center of symmetry in the monoclinic form and displaying large thermal parameters. Some ordering of these cations might be responsible for the observed superstructure.

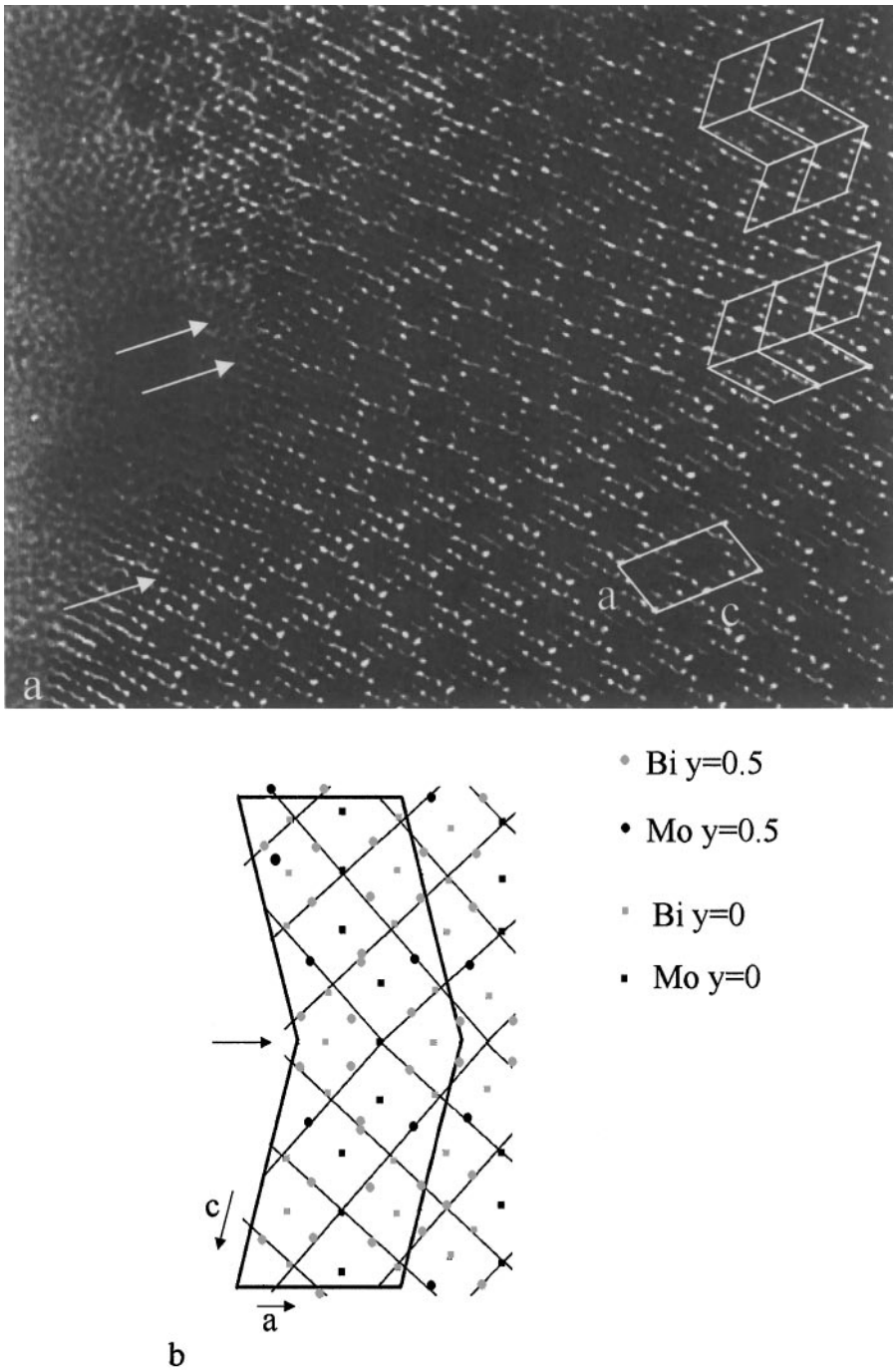

FIG. 8. $Bi_{26}Mo_{9.6}Bi_{0.4}O_{68.4}$: (a) The [010] high-resolution image: twin boundaries are often observed (arrows). (b) Schematic representation of these twin boundaries.

ACKNOWLEDGMENTS

The authors sincerely thank Professor G. Van Tendeloo for interesting and useful discussions and the EMAT laboratory (Antwerp, Belgium) for microscopy facilities.

REFERENCES

1. R. N. Vannier, G. Mairesse, F. Abraham, and G. Nowogrocki, *J. Solid State Chem.* **122,** 394–406 (1996).
2. D. J. Buttrey, T. Vogt, U. Wildgruber, and W. R. Robinson, *J. Solid State Chem.* **111,** 118–127 (1994).

3. D. J. Buttrey, D. A. Jefferson, and J. M. Thomas, *Philos. Mag. A* **53**(6), 897–906 (1986).
4. D. J. Buttrey, D. A. Jefferson, and J. M. Thomas, *Mater. Res. Bull.* **21,** 739–744 (1986).
5. D. J. Buttrey, T. Vogt, G. P. A. Yap, and A. L. Rheingold, *Mater. Res. Bull.* **32**(7), 947–963 (1997).
6. R. Enjalbert, G. Hasselmann, and J. Galy, *J. Solid State Chem.* **131,** 236–245 (1997).
7. R. N. Vannier, F. Abraham, G. Nowogrocki, and G. Mairesse, *J. Solid State Chem.* **142,** 294–304 (1999).
8. P. Stadelman, EMS: Electron Microscopy Image Simulation.
9. J. I. Goldstein, D. B. Williams, and G. Cliff, *in* "Principles of Analytical Electron Microscopy" (D. C. Joy, A. D. Romig, Jr., and J. I. Goldstein, Eds.), p. 155. Plenum, New York/London, 1986.
10. E. Van Capellen and J. C. Doukhan, *Ultamicroscopy* **53,** 343–349 (1994).
11. C. D. Ling, R. L. Withers, S. Schmidt, and J. G. Thompson, *J. Solid State Chem.* **137,** 42–61 (1998).
12. J. P. Morniroli and J. W. Steeds, *Ultramicroscopy* **45,** 219–239 (1992).